Surface & Coatings Technology 462 (2023) 129508

Contents lists available at ScienceDirect

Surface & Coatings Technology

journal homepage: www.elsevier.com/locate/surfcoat

Effect of heat treatments on the wear resistance of HVAF and HVOF sprayed tool steel coatings

Tommi Varis [a,*], Juha Lagerbom [b], Tomi Suhonen [c], Lassi Raami [a], Sakari Terho [d], Jussi Laurila [a], Pasi Peura [a], Petri Vuoristo [a]

[a] Tampere University, Faculty of Engineering and Natural Sciences, Tampere, Finland
[b] VTT Technical Research Centre of Finland Ltd, Tampere, Finland
[c] VTT Technical Research Centre of Finland Ltd, Espoo, Finland
[d] Luvata, Pori, Finland

ARTICLE INFO

Keywords:
Three-body abrasion
Cavitation erosion
Steel
Thermal spray coatings
Wear testing

ABSTRACT

Iron-based coatings are an attractive solution for many wear applications, considering sustainability requirements such as avoidance of critical raw materials and toxic substances. Cold worked tool steels are one potential, yet very undiscovered, material option for coating applications. As a bulk, their careful heat treatment typically produces a martensitic carbide microstructure with very good wear resistance. Compared to bulk materials, the thermal history of a thermally sprayed coating in the as sprayed state is quite different as the microstructure of the sprayed coating does not form in equilibrium. This study explored the potential of AISI D2 cold worked tool steel as a thermal spray coating under different wear conditions. The study investigated different heat treatments to achieve different microstructures of the powder and coatings and their effect on the wear and cavitation erosion properties of the HVOF and HVAF sprayed thermally sprayed tool steel coating. It is important to understand whether the properties of thermally sprayed coatings, which initially have a high defect density, can be improved by heat treatments, and how modification of the phase structures of iron-based coatings affects their properties, in order to extend the use of these coatings.

1. Introduction

Iron-based thermally sprayed coatings have long been an attractive alternative to WC-Co/CoCr because of their environmental friendliness and relatively low price. They are used in several applications, particularly if corrosion resistance is required in addition to wear resistance [1]. Such applications include biomass fired boilers [2,3], steam turbine blades [4], pumps and valves [5,6], cylinder bores in car engines [7–12], and hydro power turbine components [13–15]. Iron-based coatings seem to be particularly suitable against sliding and erosion wear [16,17].

Iron-based thermally sprayed coatings have shown to possess good performance against cavitation erosion. Based on the published literature, the performance of thermally sprayed coatings appears to be based on material solutions that differ from cavitation resistant steels. In cavitation resistant (solid) steels martensitic steels have shown excellent cavitation erosion resistance and it correlates with their hardness [18–20]. However, the much softer austenitic or dual phase steels have in many cases been even better due to their strain hardening properties [21–25]. With respect to thermally sprayed coatings, there are no cavitation erosion results for martensitic iron coatings in the literature and neither the results that clearly show the effect of austenitic phase strain hardening on cavitation resistance. In general, the cavitation resistance of thermally sprayed coatings has been reported to be based on their high hardness due to the high solid solution content of carbon and carbide and boride formers, which provide high hardness due to the solid solution strengthening and/or precipitation hardening. For example, Milanti et al. [26] showed relatively good cavitation erosion performance for HVOF-sprayed Fe-Cr-Ni-C-B alloy coating and Yupin et al. [27] for HVOF sprayed Fe–Cr–Si–B–Mn coating. The concentration of Cr and C in such a material induces the formation of Cr_3C_2, Cr_7C_3, $(Cr,Fe)_{23}C_6$ and $(Cr,Fe)_2B$ precipitates. Typically high concentrations of chromium and nickel in these alloys improve corrosion resistance [28] and nickel also relatively effectively stabilizes austenite phase in the matrix [26]. A few attempts have been made to develop strain hardenable iron-based coatings. Lavigne et al. [13] used a low carbon Fe-Cr-

* Corresponding author.
E-mail address: tommi.varis@tuni.fi (T. Varis).

https://doi.org/10.1016/j.surfcoat.2023.129508
Received 15 December 2022; Received in revised form 6 April 2023; Accepted 7 April 2023
Available online 11 April 2023

Table I
Böhler K110 cold work tool steel (Wt. no. 1.2379, D2) compositional analysis.

	Fe	C	Si	Mn	Cr	Mo	V	Ni	P	S	Cu
wt%	bal	1.52	0.34	0.39	11.16	0.84	0.74	0.33	0.02	0.0003	0.09

Mn-Co-Si alloy when they studied the role of strain hardenable austenite in HVOF coating to enhance cavitation resistance. They showed that transformation was taking place, but the premature failure was caused by weak inter-splat boundaries, defects, and pores and oxides in the coatings. It was evident that the effect of the thermal spray process on the microstructure was significant.

Against abrasive wear, on the other hand, iron based coatings are clearly inferior to WC-CoCr coatings [26,29]. This is mainly because iron-based powders are typically produced by atomization and their microstructure is formed during rapid melt solidification. Because the cooling rate is relatively high, there is little time for the carbides to precipitate. Typically, no detectable carbides are found at the resolution level of the SEM [30]. Therefore, compared to WC-Co and Cr_3C_2-NiCr powders produced by agglomeration, the atomized powders have relatively low carbide content, small carbide size, and their hardness is somewhat lower than the hardness achieved using WC-Co and Cr_3C_2-NiCr powders. For this reason, iron-based coatings may not be the best option against abrasive wear.

Several metallurgical methods can be used to tailor the strength, toughness, and hardness of steels. In tool steels and high strength steels metallurgical strengthening mechanisms are based either on phase transformations that initiate strain hardening or high solid solution concentrations that induce solid solution strengthening, dispersion strengthening, and precipitation hardening. Heat treatment plays a very important role in the properties of such steels. In modern steels alloy design and their precisely heat-treated structures utilize multiple strengthening mechanisms in the same alloy, which has been shown to improve strength and ductility simultaneously. The example of dual phase materials, where several categories of strengthening mechanisms have been utilized are TWIP-TRIP (Twinning induced plasticity – Transformation induced plasticity) steels in which the simultaneous improvement in strength and ductility has been achieved by combination of several strain hardening mechanisms [31]. Another example of alloys which are strengthened using mechanisms including marked solid-solution and precipitation strengthening, deformation twinning, and the formation of ε-martensite and α-martensite phases are FeCrNi-based stainless steels or FeMnC-based TWIP steels [31]. In typical tool steels, where a good combination of hardness and toughness is sought, austenitizing and quenching are carried out to form a fine-grained martensitic microstructure with carbide precipitates. Quite often in highly alloyed tool steel the transformation of austenite to martensite does not go to completion and some prior austenite can remain leaving retained austenite in the structure. Retained austenite is typically considered as detrimental to properties of the steel. Volume fraction of retained austenite in tool steels is mostly dependent on martensite start temperature, M_{start}, which is considerably affected by the composition of the steel, especially the carbon content. [30–33]

The manufacturing process for thermally sprayed coatings can be characterized as a splat-by-splat process with very high cooling rates in individual splats. In such coating microstructures, factors such as cohesion between the resulting lamellae, interlamellar oxidation and rapid quenching influence the microstructure of the coating, and it is not at all clear that the strengthening mechanisms of the internal microstructure in the lamellae can be directly transferred to the performance of the coating [13,27]. It can be argued that new processes such as HVAF and careful optimization can bring the properties closer to solid materials. However, it is not clear how the microstructure of a thermally sprayed tool steel coating is formed and whether the strain hardening properties can be fully exploited in thermally sprayed coatings. Thermally sprayed iron-based coatings are generally not heat treated to achieve high mechanical strength, as they are not designed for structural strength but for wear and corrosion resistance. Therefore, apart from a few papers on the effect of heat treatment on the mechanical properties of thermally sprayed Fe based coatings [34–37] and the effects of powder heat treatment on coating formation [38], the benefits of heat treatment of iron based powders and coatings are not deeply discovered. The objective of this study was to study the wear and cavitation erosion properties of air hardened high chrome tool steel thermally sprayed coating and investigates the coating properties achieved by different thermal spray processes and heat treatments of the coating or powder. Of particular interest was to investigate the role of strain hardening of retained austenite on the cavitation erosion of the coating. The influence of the spraying process was also investigated by spraying the coating with High velocity oxygen fuel (HVOF) and High velocity air fuel (HVAF) processes. The research questions addressed in this study are a) how the different initial structure of the powder affects the structure of the coating, b) how the different coating methods, HVOF versus HVAF, affect the resulting microstructure, c) how different heat treatments of iron-based coatings affect the wear resistance of the coating.

Table II
The labeling of coatings from heat treatment and spray process.

Coating label indicating the spray process and treatment		Heat-treatment of the powder or coating
HVOF A	HVAF A	As-atomised Powder A, As-sprayed coating
HVOF M	HVAF M	Powder M heat treated 550 °C, 8 h in Ar 5 % H_2
HVOF A500	HVAF A500	Powder A, Coating heat-treated at 500 °C 3.5 h in Ar 5 % H_2
HVOF A600	HVAF A600	Powder A, Coating heat-treated at 600 °C 3.5 h in Ar 5 % H_2

2. Experimental

This paper focuses on the abrasion and cavitation erosion resistance of HVOF and HVAF sprayed coatings made from iron-based powder. The powders were prepared using commercial Böhler K110 cold worked steel rod (Wt. No. 1.2379, D2) as raw material. The compositional analysis of the steel is presented in Table I. K110 is a high carbon high chromium steel with high wear resistance and ductility.

The microstructure of the coatings was modified by different heat-treatments either for the powder or for the coating. The treatments carried out in the study were resulted the following coatings:

i. HVOF and HVAF coatings made of as-atomized Powder A,
ii. HVOF and HVAF coatings made of atomized Powder M, which was heat treated to transform retained austenite in the powder,
iii. HVOF and HVAF coatings made from atomized Powder A. Coatings were heat-treated at 500 °C with the purpose of ***partially*** transform the retained austenite in the coating.
iv. Heat-treated HVOF and HVAF coatings made from atomized Powder (A), where the purpose of the heat treatment was to fully decompose retained austenite in the coating.

The heat treatments and coating labeling are shown in Table II. The heat treatments and their justification are described in more detail in Section 2.3.

Table III
The spray parameters used for coating preparation.

Spray process	Propane 1	Propane 2	Oxygen	Air	Nitrogen	Stand-off distance
HVOF	70 l/min	–	238 l/min	375 l/min 7.4 bar	20 l/min	250 mm
HVAF	7.3 bar (106 psi)	7.2 bar (105 psi)	–	(108 psi)	60 l/min	300 mm

2.1. Powder preparation

Experimental powders were produced by high-pressure gas atomization, Hermiga 75/5 VI atomization unit from Phoenix Scientific Industries Ltd., East Sussex, UK with Ar-gas. The atomizer included induction melting furnace and bottom-pour tapping crucible. The configuration was close-coupled atomization die/guide tube for fine particle size and controlled particle size distribution. During atomization, 5 kg batch of the alloy was inductively melted and the melt overheated for 200 °C to ensure melt flow. The melt was then fed at 0.25 bar overpressure into a melt nozzle with diameter of 2 mm. The melt flow was atomized to droplets by laminar atomization nozzle with 60 bar argon gas. Gas to melt ratio was 3.5. The droplets rapidly solidified in the atomization chamber into spherical particles at 10^5–10^6 °C/s. The solid, larger powder particles collect in a hopper below the atomization chamber. Fine particles travel with the gas flow and are separated in a cyclone. In this case, only the chamber fraction was used in thermal spraying due to its suitable particle size distribution.

Atomized powder was sieved with 45 μm aperture sieve for HVOF and 32 μm aperture sieve for HVAF spraying. Separation of fines during atomization was adequate and no fines were necessary to be removed from the feedstock. Particle sizes were measured by Malvern Master sizer 3000 (Malvern Panalytical, UK) laser diffraction analyzer. Part of the powder was heat treated at 550 °C for 8 h and cooled. The justification for the heat treatments is given in Section 2.3.

2.2. Coating preparation

Coatings were sprayed using high kinetic processes. HVOF gun was Diamond Jet Hybrid 2700 (propane) from Oerlikon Metco AG (Wohlen, Switzerland) and HVAF gun was M3 from Uniquecoat Technologies LLC (Oilville, USA). The DJ Hybrid used a standard propane configuration with a 2701 de Laval nozzle. The M3 used propane as fuel gas and the gun was equipped with a short combustion chamber and a de Laval nozzle labelled as 4L2. Details of the spraying parameters are given in Table III. Coatings were applied on (150 × 50 × 5) mm steel substrate using a robot with 0.9 m/s traverse speed and a step width of 4 mm. The substrate temperature was monitored during spraying with a Fluke Ti300 (Everett, WA, USA) thermal imager, which allowed the temperature of the sample to be kept at approximately 200 °C. The powder feed rate was 40 g/min, which kept the coating build-up below 17 μm/pass.

2.3. Heat treatment procedures

With the purpose of improving the lamellae adhesion, forming of secondary carbides and decomposing the retained austenite the tempering procedures for the powder and coatings were designed based on the Time-Temperature-Transformation and Tempering diagrams from the steel manufacturer's datasheets shown in Fig. 1a and b. However, the TTT diagram does not fully describe the situation of the thermally sprayed coatings, because their microstructure is formed of very rapidly quenched splats with a cooling rate of 10^6–10^9 °C/s whose microstructure does not reach equilibrium.

The thermal history of tempered coatings is described as follows. During the thermal spray process, the powder particles quenched directly from a high temperature, which can be molten, semi-molten or very close to molten depending on the particle size, to a substrate temperature of about 200 °C. Two as-sprayed coatings were tempered for 3.5 h at 500 °C and 600 °C in an argon atmosphere. The samples were heated to an isothermal tempering temperature at the rate of 3.5 °C/min. With such a slow heating rate, it is likely that bainite nose was crossed and some of the retained austenite decomposes to lower bainite. During the isothermal tempering the precipitation of carbides takes place, which reduces the carbon content in the austenite. The decrease in the carbon content of austenite during tempering increases the martensite start (M_{start}) and martensite finish (M_{finish}) temperatures so that, on subsequent cooling at 5 °C/min, the retained austenite transforms to martensite. The carbon content remaining in the austenite and hence the M_{finish} temperature practically determines how much residual austenite remains after this treatment. The heat treatment of the coating at 500 °C was aimed at lowering the carbon content in the austenite by the formation of carbides to such an extent that the M_{start} temperature would be above room temperature but the M_{finish} temperature below room temperature. This treatment targeted to form a partly martensitic/

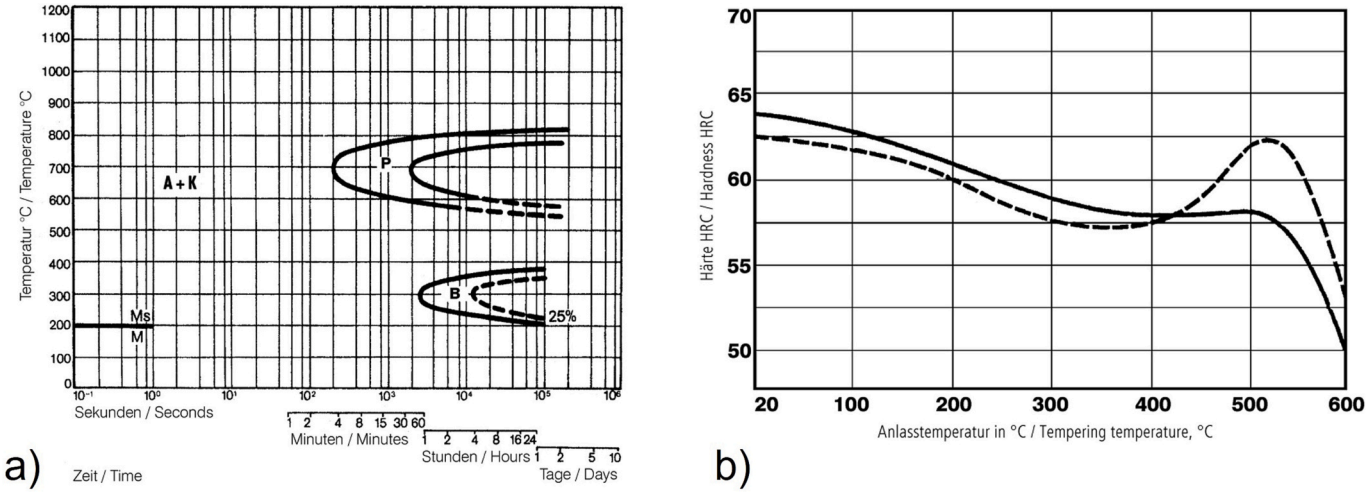

Fig. 1. a) Isothermal Time-temperature-transformation (TTT) curve based on austenitizing temperature of 1020 °C for 30 min and b) tempering chart of the K110 steel where dashed line for hardening temperature of 1070 °C and the solid line 1030 °C.

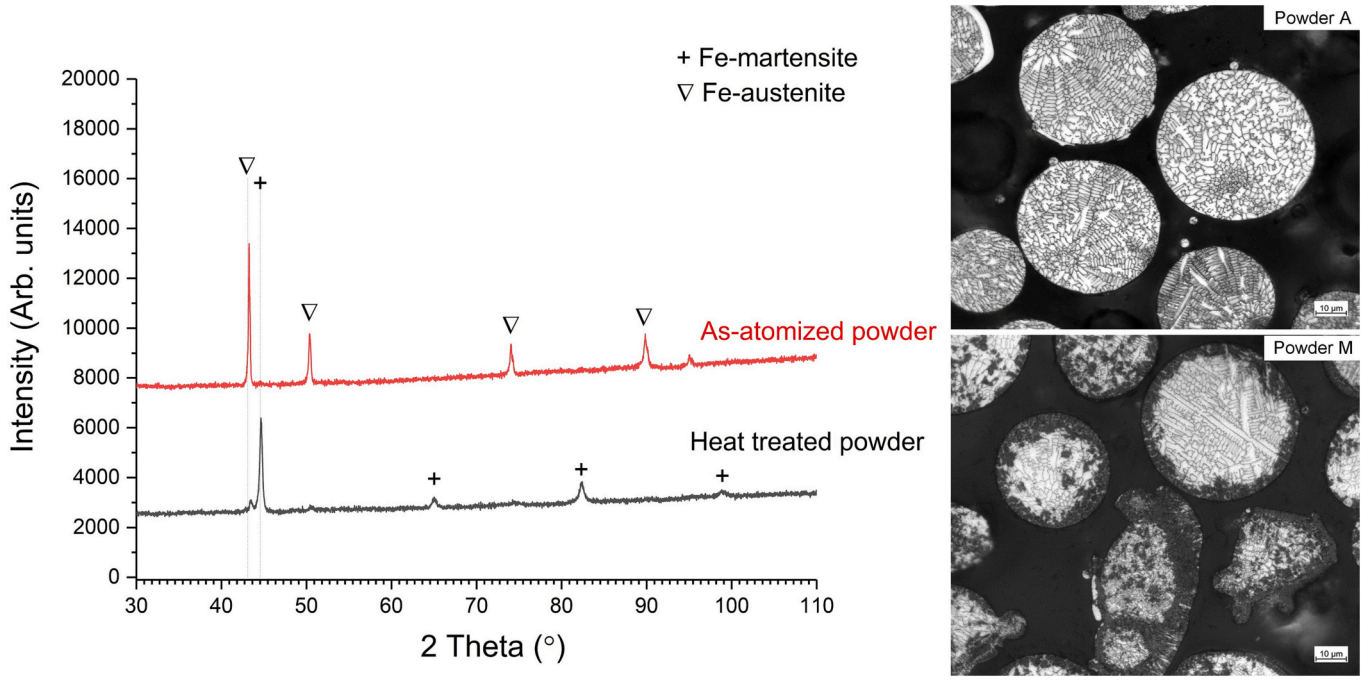

Fig. 2. XRD-analysis and cross section microstructures of the powders (Powder A upper and Powder M below). Powders were etched with Nital to reveal the microstructure. Powder A show a mixture ledeburitic structure while powder M have etched martensite outer rim.

bainitic and partly retained austenitic structure. The heat treatment of the coating at 600 °C was aimed at further increasing the carbide content and increases their size during tempering. According to the TTT curve, this temperature is at the region of perlite, and it is likely that perlite will also form with the carbides during the treatment at 600 °C.

For the powder the tempering at 550 °C was chosen which, according to the tempering diagram, gives hardness increase explained by the precipitation of the secondary carbides. Also, in the case of powder the bainite formation during the heating at the rate of 3.5 °C/min. During the subsequent cooling at the rate of 5 °C/min the remained retained austenite would transform to martensite. To verify the microstructure produced by the heat treatment, a preliminary test was carried out in which a small amount of powder was heat treated at 550 °C for 2 h in an Ar atmosphere. The microstructure and phase composition of powder M was determined for a powder subjected to the heat treatment of this preliminary study.

2.4. Coating and powder characterization

For structural studies, cross-sectional specimens of the coating and powders were prepared by casting in resin, grinding and mechanical polishing. The polished cross-sectional samples were characterized with a JSM-IT500 (JEOL, Tokyo, Japan) scanning electron microscope (SEM) in backscattered electron (BSE) mode using a 15 kV acceleration voltage and a working distance of approximately 10 mm. Coating Vickers harnesses were measured using an Emcotest hardness tester by Struers, Kuchl, Germany. Hardness was measured on the polished cross sections under a 300 g load. Ten indentations were performed on each coating. The phase compositions of the powders and the coatings were determined by Empyrean x-ray diffractometry (Malvern Panalytical, Almelo, The Netherlands) using Cu-Kα radiation (1.5406 Å, 40 kV and 45 mA). Phase identification was done with HighScorePlus software (Malvern Panalytical, Almelo, The Netherlands). The coating phases were visualized by electron backscatter diffraction (EBSD) measurements, which were performed using ZeissUltra Plus (Carl Zeiss AG, Oberkochen, Germany) UHR FESEM microscope with the HKL Premium-F Channel EBSD ultrafast Nordlys F400 detector provided by Oxford Instruments, Bucks, England. For EBSD cross-sections were polished by ion-milling with IB-19530 Cross Section Polisher (JEOL, Akishima, Japan).

2.5. Wear testing

Cavitation erosion wear resistance of the samples was tested according to ASTM G32-16 “Standard Test Method for Cavitation Erosion Using Vibratory Apparatus”. In the test, samples of 25 × 25 × 5 mm size, ground with grit 4000 sandpaper, were placed in distilled water and a high-frequency vibrating tip was placed at 500 μm distance from the sample. The tests used a VCX-750 ultrasonic transducer from Sonics & Materials, USA, which vibrates at a frequency of 20 kHz and an amplitude of 50 μm, causing bubbles to form and collapse in the fluid, and the collapsing bubbles caused damage and erosion (loss of material) of the sample. The vibration tip was an alloy of Ti-6Al-4 V, and tip diameter was 15.9 mm. Water temperature was kept at 25 °C. The samples were weighed with high accuracy scale after 15, 30, 60, 120, 240, and 360 min. Prior to weighing the samples were cleaned in an ultrasonic bath with ethanol and dried.

Abrasion wear behavior of the coatings was evaluated using a modified version of the ASTM G65 dry sand–rubber-wheel abrasion wear test, where five samples were tested simultaneously. Blocky-shaped dry quartz sand (SiO_2) with a grain size ranging from 0.1 to 0.6 mm was used as the abrasive. The flow rate of the abrasive was 25 g/min. Sample surfaces were ground using grit 600 SiC paper before testing. During the test, the samples were pressed with a normal load of 23 N against a rotating rubber wheel which had a surface speed of 1.64 m/s. The 60 min test time used gives a wear length of 5904 m. The samples were weighed every 12 min using a high accuracy scale.

3. Results and discussion

3.1. Powder characteristics

Particle size of the HVOF powder was D_{10} 19, D_{50} 33, and D_{90} 52 μm and HVAF powder D_{10} 15, D_{50} 24, and D_{90} 38 μm. Two different batches of this powder were used in the spraying experiments. One of the

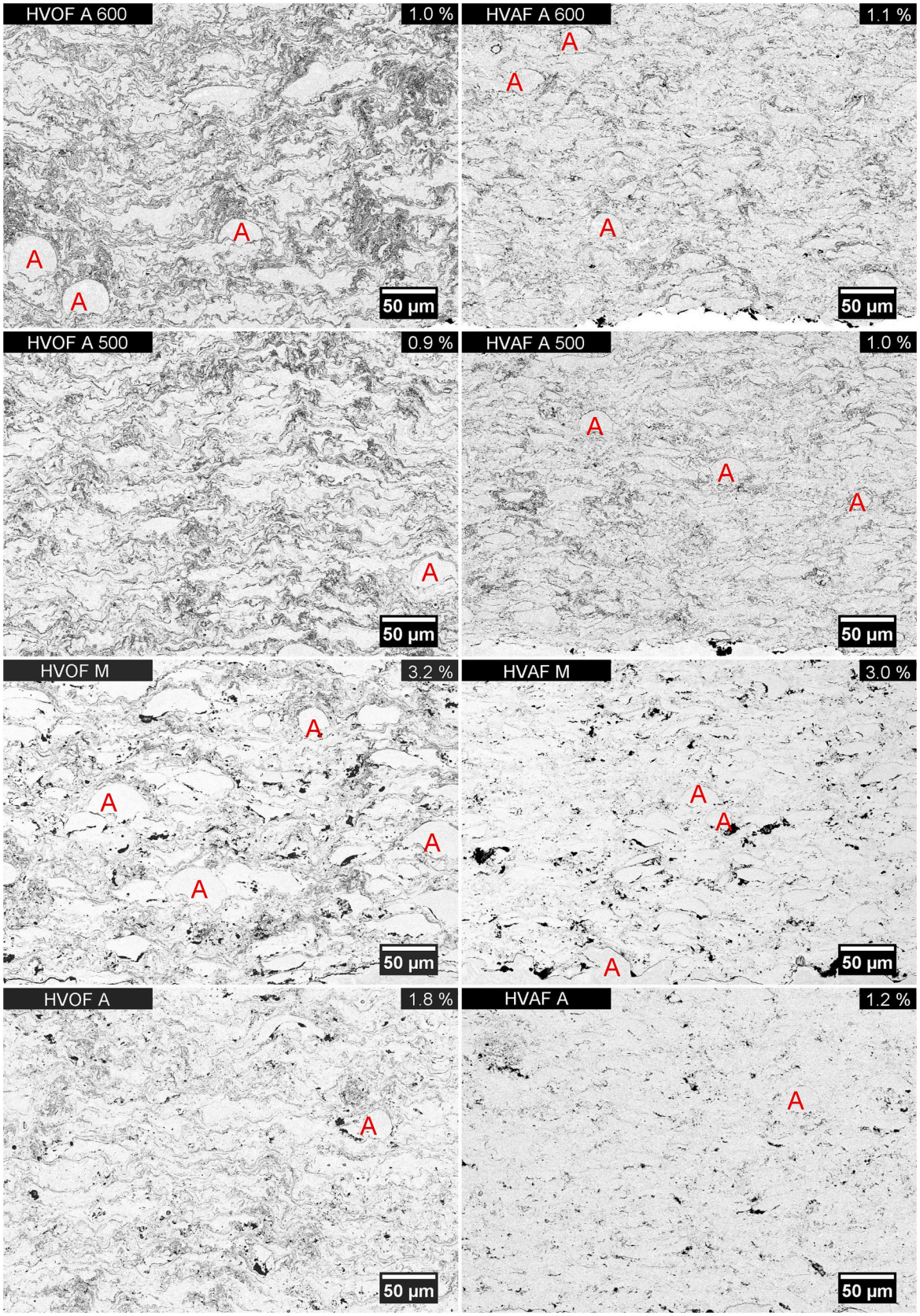

Fig. 3. Microstructures of coatings, with some of the non-melted or not fully melted particles marked with A. The porosity of the coatings is shown in the upper right corner of the image.

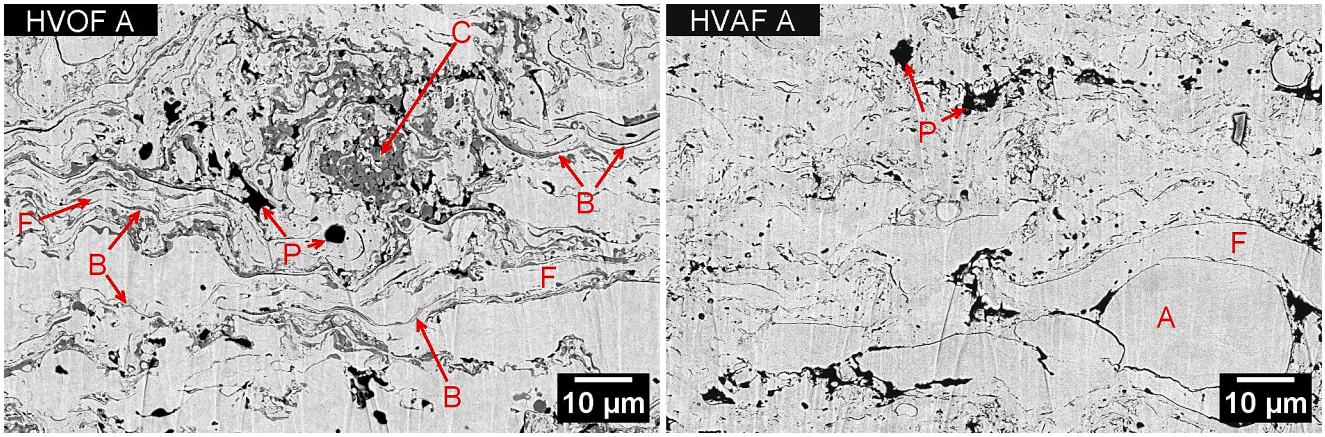

Fig. 4. Cross sectional images of the HVOF A and HVAF A coatings polished by ion-milling. Some features of the coatings indicated by: A non-melted splat, B lamellar oxide bands, C oxide clusters, F well flattened splat, and P porosity.

powders, powder A, was directly formed by atomization process (as atomized). Another batch of powder, powder M, which was tempered at 550 °C.

Fig. 2 presents XRD and cross section of the as-atomized powder particles which have mixture of dendritic features and cellular morphology, which is likely to be controlled by cooling rate [33]. XRD reveals only austenite (FCC) peaks, but it is likely that highly etched darker regions, which surround the austenite grains, are carbide eutectic, in this case $(Cr,Fe)_7C_3$ [39]. Carbide eutectic is formed as austenite and carbide solidify eutectically from the melt into the interstitial spaces of already crystallized austenite. This carbide eutectic is very fine structures and cannot be seen at the resolution of the image.

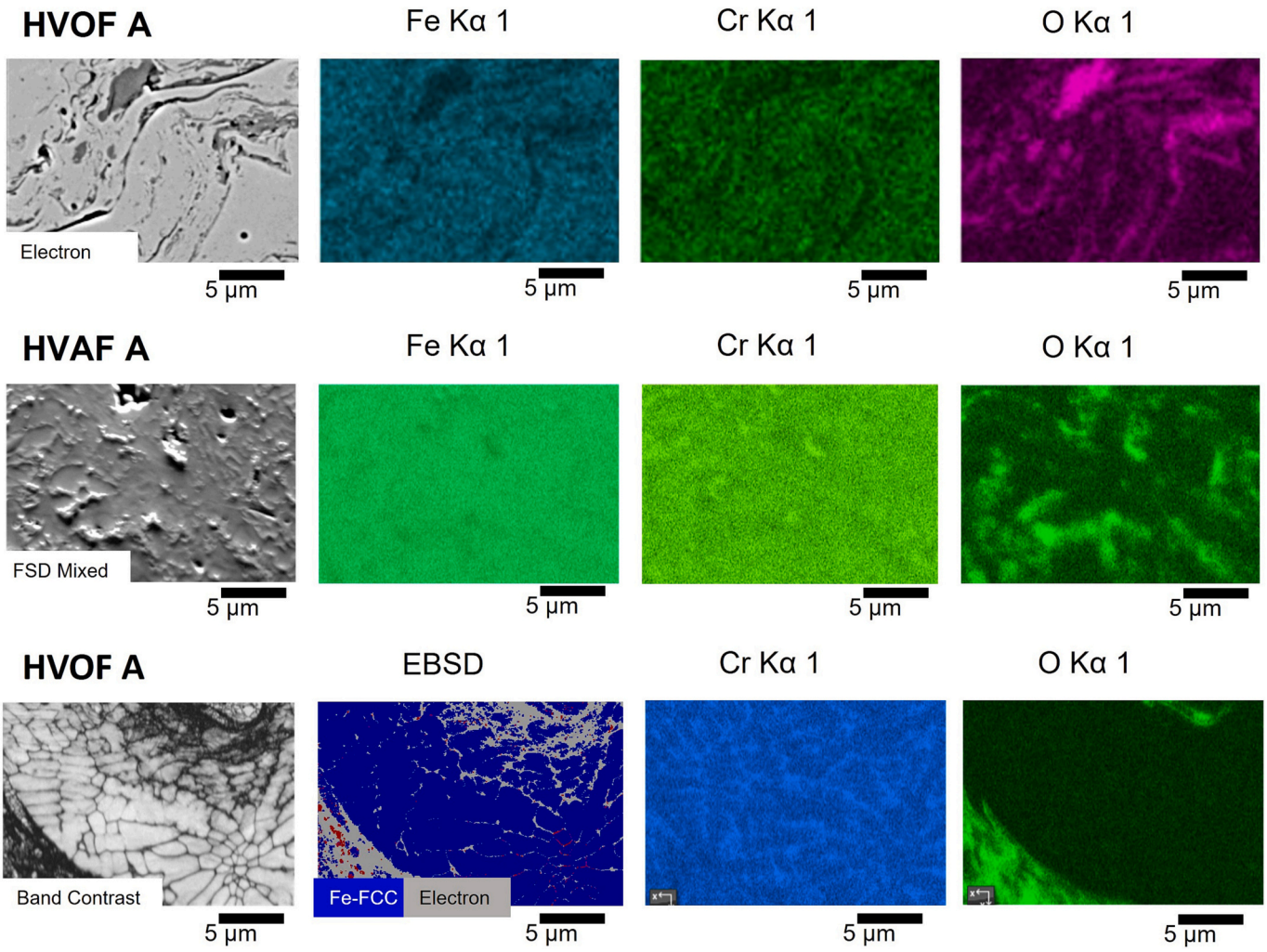

Fig. 5. EDS elemental mapping showing the Cr and O in the HVOF A (top) and HVAF A (middle). The bottom row shows the phase structure of the non-melted particle and the Cr and O distributions in the HVOF A coating.

However, such a structure can be seen in the non-melted particle of coating HVOF A in the bottom row of Fig. 5. Austenite, the light phase in the image (verified by the XRD), was retained and martensite formation was prevented due to high alloying (especially high carbon content) and high cooling rates. As a result, carbon and other alloying elements were super-saturated in solid solution.

Looking at the microstructure of the powder tempered at 550 °C for 2 h in Fig. 2, it is observed that the outer shell of the powder particles is strongly etched. XRD pattern of the powder from preliminary test shows no evidence of austenite. This suggests that there is a martensitic/bainitic shell on the surface of the powder. In theory, transition carbides are formed, and austenite is depleted of carbon, which contribute to formation of martensite during air cooling of the powder. During the heat up phase, the formation of bainite is also possible. The formation of a martensitic/bainitic structure only on the outer shell of the powder particles indicates that the 2 h tempering time used in the preliminary test was not sufficient for the austenite decomposition throughout the powder particles, so treatment time was increased to 8 h for the actual powder tempering to fully decompose the retained austenite in the powder.

3.2. Coating characteristics

The microstructures and resulting phases of the coatings prepared according to Table II were analyzed by hardness measurements, SEM imaging, optical microscope imaging from etched surface, and EBSD. The coatings were further examined by etching them with 3 % Nital, which highlights pores and lamellar boundaries in TS coatings. More importantly etching reveals martensitic structures or chromium-depleted areas, which tend to be more easily etchable. It should be mentioned that the etchings are not fully comparable, as the etching times may not be exactly same.

The SEM microstructures of the coatings and the porosity measured with Image J in Fig. 3 reveal the typical features of sprayed coatings. It can be observed that some non-melted or incompletely melted particles remain in the coatings, which are indicated by A in Fig. 3. The problem with non-melted particles is that if the powder particle does not melt completely, its flattening upon impact is limited and the particle cannot fill the irregularities in the underlying coating. Consequently, pore pockets are easily formed around non-melted particle, which creates pore pockets that cannot be filled by subsequent particles either and filling becomes incomplete. Porosity caused by non-melted particles is particularly observed in martensite powder coatings, HVOF M and HVAF M. The poor deformation ability of martensite powder due to its high strength further contributes to the problem. It is notable that both heat-treated coatings, at 500 °C and 600 °C, have a lower porosity than as-sprayed coatings. This suggests that the heat treatment increases the adhesion between the lamellae and thus the cross-section sample preparation does not produce as many pull-outs.

Another typical defect in thermally sprayed coatings is oxidation, which was evident in both HVOF and HVAF coating. Oxidation occurred differently in HVOF and HVAF coatings, which is shown in micrographs in Fig. 4 and elemental analysis in Fig. 5. In HVOF coating the degree of inflight oxidation is higher compared to HVAF obviously due to its higher flame temperature. In HVOF coatings, oxides appear either as narrow oxide bands surrounding lamellar splat (B in Fig. 4) or as oxide clusters (C in Fig. 4). Oxide clusters are composed of oxidized particles initiated from fractured oxide bands, oxidized fine particles or splashes. Oxidation naturally occur only on the surface of the particle thus non-melted particles form non-oxidized region in the coating, which corresponds to the structure of the original powder particles as observed in Fig. 5 for HVOF A. The etching of the HVOF A coating, in Fig. 9, also reveals the original ledeburite eutectic carbide structure in non-melted particles. Oxides in HVAF coatings were found to occur differently. EDS elemental mapping in Fig. 5 shows that in the HVAF coating, the oxides are not lamellar but like dispersions in the regions between the

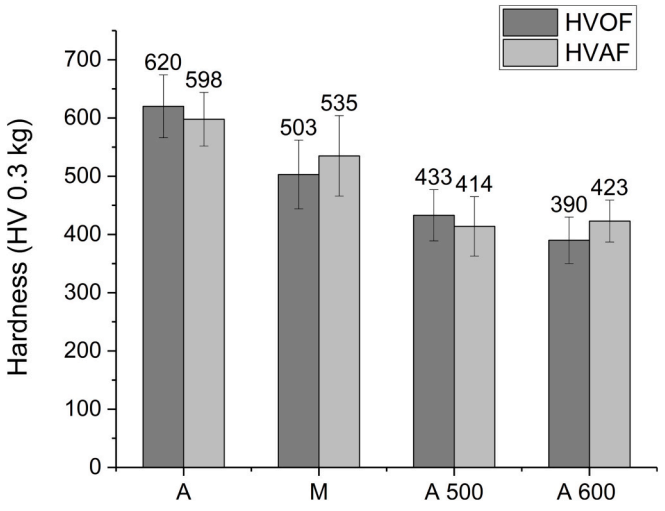

Fig. 6. Hardness's of as sprayed HVOF and HVAF coatings from austenitic powder A, martensitic powder M, coating heat treated at 500 °C (A500), and coating heat treated at 600 °C (A600).

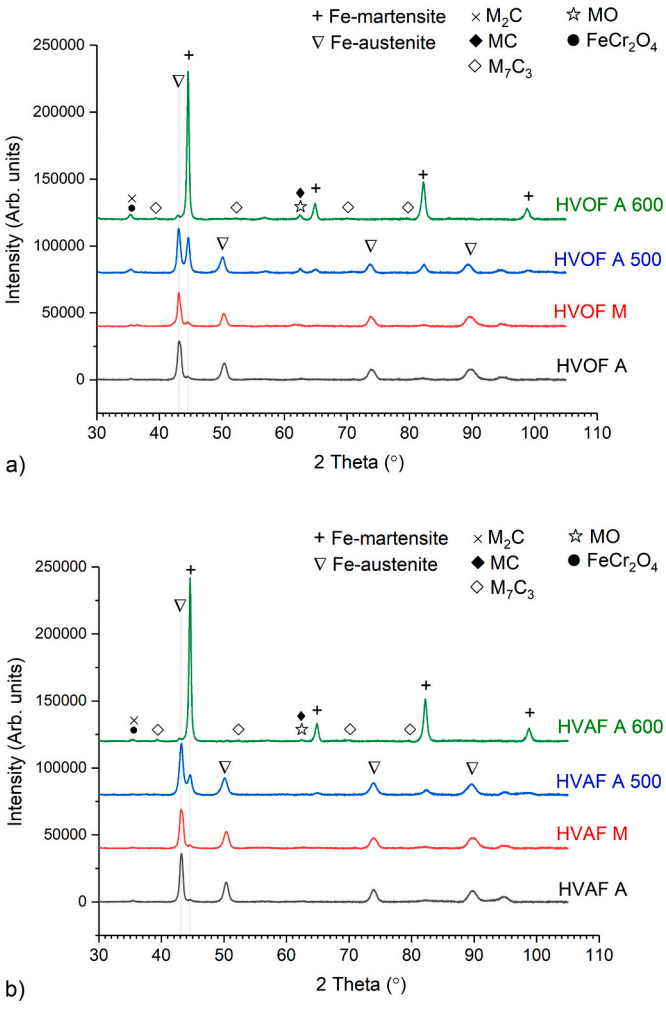

Fig. 7. XRD patterns of the a) HVOF and b) HVAF coatings. The deposition process and powder/coating indicated in the right of the corresponding pattern.

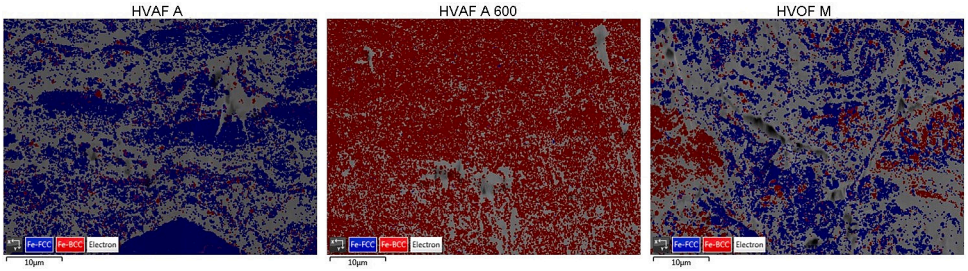

Fig. 8. EBSD analysis of the HVAF A, HVAF A600, and HVOF M coatings. Blue color showing Fe-FCC (Austenite) and red color Fe-BCC (Martensite/Ferrite).

splats. It is possible that the thin oxide layer formed on the surface of the particle during HVAF spraying has already solidified before the impact and therefore does not form banded structures but breaks up into small fragments on impact.

Despite the high oxide content visible in the microstructures of especially HVOF coatings, no oxide peaks are observed in the XRD pattern of the as sprayed coatings. In the XRD pattern, peaks are observed, which could be identified as $FeCr_2O_4$ (2-theta of 35.1°) and MO (2-theta of 62.7°), but they cannot be confirmed as oxides because they are at the same theta angles where carbides also occur. The absence of oxide peaks strongly suggests that the rapidly quenched oxides formed during spraying are amorphous. The formation of amorphous oxides in iron based thermally sprayed coatings and their effect on mechanical properties has been reported by Rabiei et al. [8] whose observations support this claim.

The hardness of the coatings, shown in Fig. 6, were 620 HV (0.3 kg) for HVOF A and 598 HV (0.3 kg) for HVAF A. The peak observed in the X-ray diffraction pattern at about 2-theta of 43.1° in Fig. 7 indicates that these as sprayed coatings were mostly retained austenite. A small peak at 2-theta of 44.5° suggests that a minimal amount of hardened martensite has also formed in the coatings. It was observed that there are no carbide peaks in the XRD pattern, and it was clear that the rapid quenching of the particles in thermal spraying inhibited the precipitation of primary carbides such as $M_{23}C_6$ and M_7C_3. EBSD images of the HVAF A coating, in Fig. 8, confirms that predominant iron phase was austenite. It is also noteworthy that EBSD analysis shows a large proportion of unidentified phases. Some of the unidentified phases appear to be in areas where EDS maps show high oxide concentrations and are therefore identifiable as Fe and Cr oxides. It can also be assumed that some of the austenite phases in the coating are distorted by supersaturated atoms and thus cannot be identified as austenite by EBSD. This is also supported by the very high hardness of coating with retained austenite especially HVOF A and HVAF A. The probable reason for the high hardness is that the distorted, supersaturated solid solution of residual austenite has a very high hardness compared to normal austenite due to the effect of the solid solution, high dispersion density and fine grain size. As can be seen in Fig. 8, the austenitic phase is well detectable by EBSD in the non-melted particle. The problem with EBSD is more evident with well melted particles, in which both the dissolution of carbides into austenite and high quenching stresses can distort the atomic lattice.

According to XRD, the phase structures of HVOF M and HVAF M coatings were predominantly austenitic, despite the martensitic starting structure of the powder. Also, no carbide-identifiable peaks were observed in XRD pattern. This indicates that when the powder particles with a martensitic structure melt during its flight, the carbides at least partially dissolve and increase the carbon content of the matrix, leaving the M_{start} temperature below room temperature and the quenched structure austenitic. However, EBSD analysis in Fig. 8 reveals that the non-melted particles in HVOF M coating remained martensitic. Furthermore, the etched microstructure of the HVOF M and HVAF M coatings showed that the etching had a strong effect on the non-melted particles in Fig. 9. These observations indicate that the original martensitic structure of the powder is preserved when the powder particle has not melted during the spraying process. It is obvious that since the powder particle did not melt, the carbides formed during the heat treatment of the powder could not dissolve during spraying. Consequently, the iron matrix in such a non-melted particle is martensitic. When comparing the hardness of HVOF M and HVAF M predominantly austenitic and HVOF A and HVAF A mainly austenitic structures, A is found to be slightly harder. However, the hardness of M coatings is very high for austenite. The lower hardness of M coatings compared to A coatings was probably due to their higher porosity caused by non-melted particles, as discussed earlier.

Isothermal tempering of the coatings at 500 °C for 3.5 h was performed well below the transformation region of perlite and above the transformation region of bainite. However, as mentioned earlier formation of lower bainite is likely as the temperature during the lifting phase crosses the bainite nose. During the isothermal tempering the formation of secondary carbides becomes possible leading to a reduction of carbon in austenite and bringing the M_{start} temperature above room temperature and the M_{finish} temperature below room temperature to achieve a partly martensitic/bainitic and partly austenitic structure. The desired structures were obtained as the XRD patterns showed a ratio of austenite to martensite/ferrite of approximately 55/45 in HVOF A500 and approximately 70/30 in HVAF A500. The XRD pattern shows the formation of eutectic M_2C and more vanadium-rich MC carbides in both coatings. As a result of the heat treatment the hardness of HVOF A500 and HVAF A500 has slightly decreased compared to as sprayed coatings, which may be explained by the structural changes in austenite. The decrease in hardness is understandable because of structural changes and homogenization of supersaturated austenite.

Tempering at 600 °C for 3.5 h is close to perlite nose, so it is likely that during this time austenite decomposes partly to perlite during tempering and partly to martensite on cooling. This is also indicated by the lower hardness compared to the coatings heat treated at 500 °C. EBSD in Fig. 8 confirms that the retained austenite is mainly decomposed. In Fig. 9, the etched structure of the heat-treated HVOF A600 and HVAF A600 coatings shows enlarged globular carbides around which the chromium-poor areas are effectively corroded. Some of the carbides in these coatings could be identified as M_2C and MC types of carbides by XRD, but also low intensity M_7C_3 carbide peaks are visible especially in the XRD pattern of HVAF A600 coating. The coatings heat-treated at 600 °C (HVOF A600 and HVAF A600) were likely to contain fine eutectic carbides and, in places, larger globular M_7C_3 carbides, in a matrix containing perlite and martensite.

3.3. Wear performance

The abrasive wear resistance of coatings presented in Fig. 10a was logically dependent on the microstructure of the coating. It was evident that the best abrasive wear resistance was achieved with the heat-treated HVOF A600 and HVAF A600 coatings, which contained eutectic carbides and, in places, larger globular carbides in a matrix containing perlite and martensite. It was observed that heat treated at 600 °C, the wear resistance of the coatings improved despite the

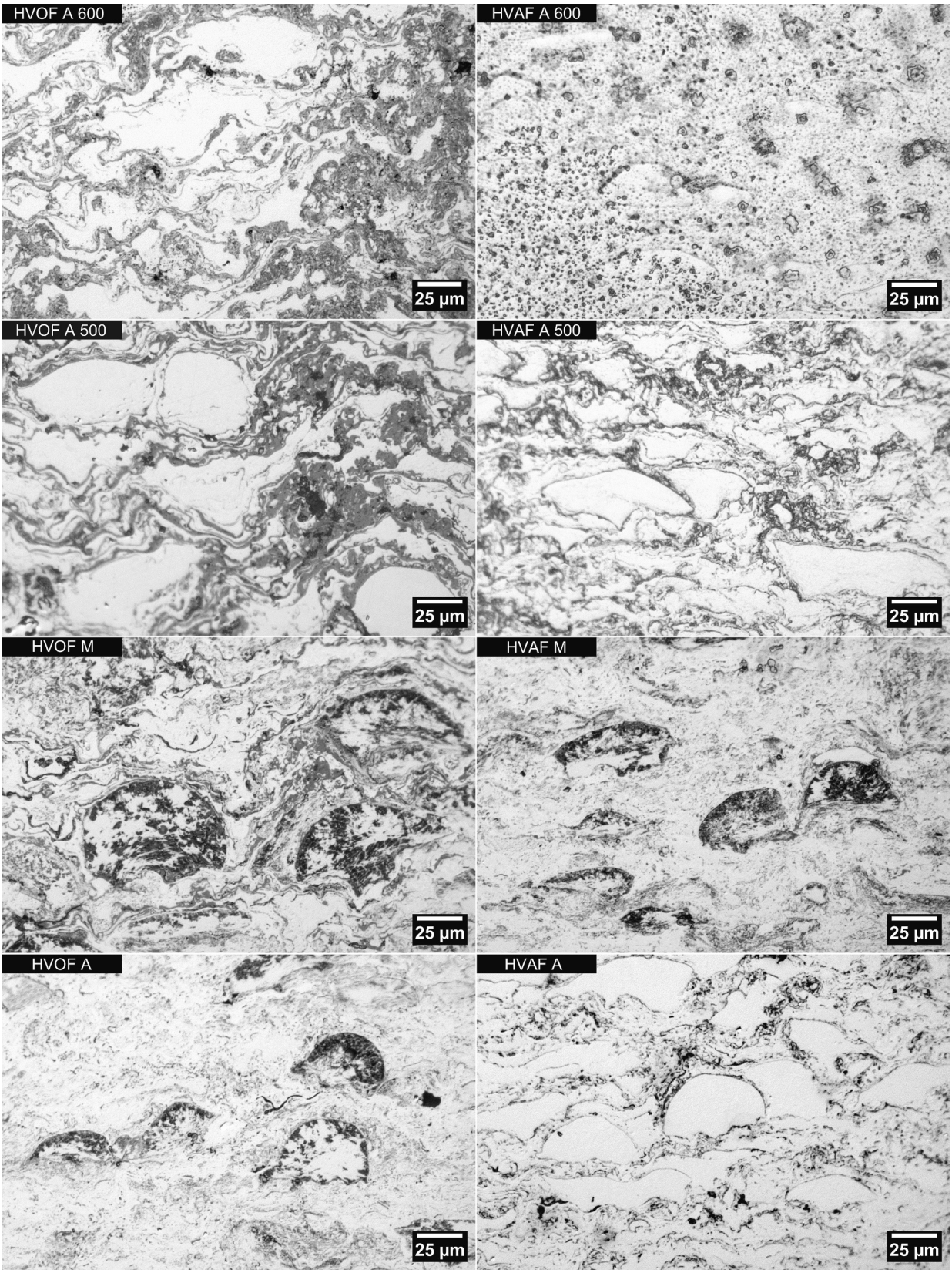

Fig. 9. Etched (nital 3 %) cross sections of the coatings by optical microscope.

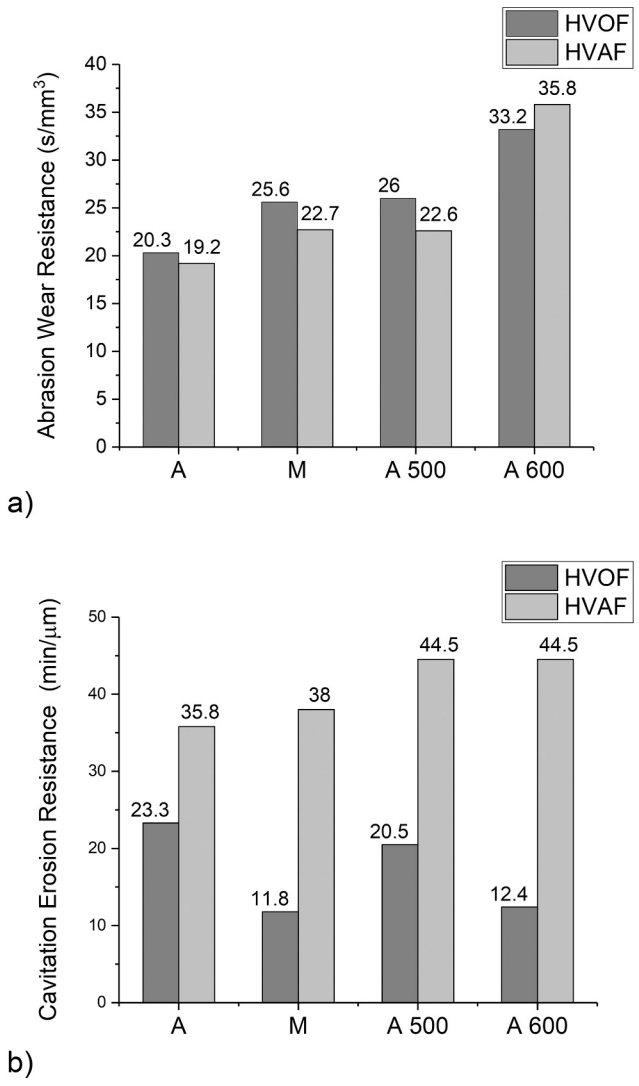

Fig. 10. a) Abrasion wear resistance of coatings in seconds/mm and b) cavitation erosion resistance of coatings in minutes/mm.

decrease in hardness compared to non-heat-treated coatings. Typically, a decrease in hardness leads to a decrease in wear resistance, so the improvement in wear resistance caused by heat treatment in this case is affected by other changes in the coating, such as an increase in carbide size or improved lamellar cohesion. It is worth mentioning that the heat treatment at 500 °C followed by only a slight increase in martensite content could not significantly increase the wear resistance of HVOF A500 and of HVAF A500. Heat treatment is often not possible and unfortunately it appears that the as sprayed coatings HVOF A and HVAF A, which produce supersaturated and almost entirely austenitic structure, do not offer good abrasion resistance despite their comparatively high Vickers hardness. HVOF M and HVAF M coatings made from martensite-treated powder achieve slightly better abrasion resistance, being at the same level as coatings heat-treated at 500 °C. Even in these coatings, the structure was mainly austenitic. However, these coatings contained non-melted particles or a heat-treated structure that was martensite with precipitated carbides, which may play a role in improving the wear resistance.

Cavitation erosion results of coatings, which were determined from the steady-state wear regime with linear erosion rate, are shown in Fig. 10b. For comparison, ASTM G32 cavitation resistances given for the corresponding D2 bulk steel are about 11 min/µm for normalized sample and about 67 min/µm for sample quenched (not tempered) from 990 °C in oil [40]. Fig. 11 shows the cavitation eroded surfaces of the coatings, which have all lost their original polished surfaces. Three main types of surfaces, shown in Fig. 12, occur on cavitation eroded surfaces: 1) smooth splat surfaces (S), 2) un-melted particles (A), and 3) rough cavitation fractured surfaces by fatigue (R). Results clearly show that HVAF coatings achieved better cavitation erosion resistance than HVOF coatings in all cases. The cavitation craters, shown in Fig. 11, are generally wider and deeper in HVOF coatings than in corresponding HVAF coatings. The existence of smooth fracture surfaces suggests that under cavitation the detachment of coating occurs relatively easily in the direction of the coating plane along the smooth lamellar boundaries of well-melted lamellae on which the next impacted particle cannot adhere well. Such smooth fracture surfaces are seen more in the HVOF A coating than in the HVAF A coating. This may also highlight the negative role of oxidation, as incoming particles do not adhere well to an oxidized smooth surface and provide favorable pathways for fatigue crack growth. Oxides, which proved as amorphous also have low local fracture toughness, so cracks propagate easily along oxidized interfaces, as also suggested by Rabiei et al. Oxidized lamellas are particularly visible in the cross-section of the HVOF A coating in Fig. 3, which may contribute to its poorer cavitation erosion resistance than the corresponding HVAF coating.

Another significant area of poor adhesion of the coating appears to be the presence of non-melted particles around which material has been removed. Delamination also seems to proceed easily along the surfaces of non-melted particles in the depth direction of the coating. The number of non-melted particles on the surface is higher for the HVOF A coating than for the HVAF A coating. HVOF M coating sprayed using martensitic powder has a particularly high number of non-melted particles, which explains the poor cavitation performance of the coating. The high number of non-melted particles in the coating is presumably due to the heat treatment, which increase the melting temperature of iron matrix. This is because the formation of carbides in the powder during heat treatment reduces the carbon content of the matrix. The reduction of carbon allows the formation of a martensitic structure during quenching, but on the other hand, as the carbon content of austenite decreases, its solidus temperature increases according to the Fe—C equilibrium diagram. Consequently, melting of the iron matrix in the heat-treated powder is more difficult and thus some of the larger particles may remain only partially melted in the coatings. In addition to having a higher melting temperature, they also harden significantly during the heat treatment, making it more difficult to deform them.

A coarser fracture surface is typically generated by the growth mechanism of a ductile fatigue crack through the lamellae in the depth direction. This mechanism is particularly prevalent in heat-treated HVOF A600 and HVAF A600 coatings. Some smooth lamella boundaries can be seen on the fracture surface of HVOF A600, but the non-melted particles are non-existing. It is likely that the absence of cavitation fracture surfaces caused by non-melted particles is explained by the improved adhesion of these non-melted particles as a result of heat treatment thus the interfaces of the non-melted particles do not act as a primary crack growth path. It is noteworthy that the heat treatment improves the cavitation resistance of the HVAF A600 coating and worsens the cavitation resistance of the HVOF A600 coating. Looking at the microstructures of the etched coatings in Fig. 9, it can be observed that HVOF A600 coatings (also HVOF A500 coatings) have areas where oxidation bands and martensite clusters are visible. It is likely that the cavitation crack in such a structure can easily propagate deeper into the material along these brittle areas, forming deep cavitation craters as seen in the HVOF A600 coating in Fig. 11.

It is known that materials such as austenitic steels with high strain hardening coefficients resist cavitation erosion well because the phase change at the crack tip prevents crack propagation [22]. No conclusions can be drawn from this study about the differences between austenitic coatings and martensitic coatings. The comparison is difficult because the coatings in the austenitic phase were in the as-sprayed state and the

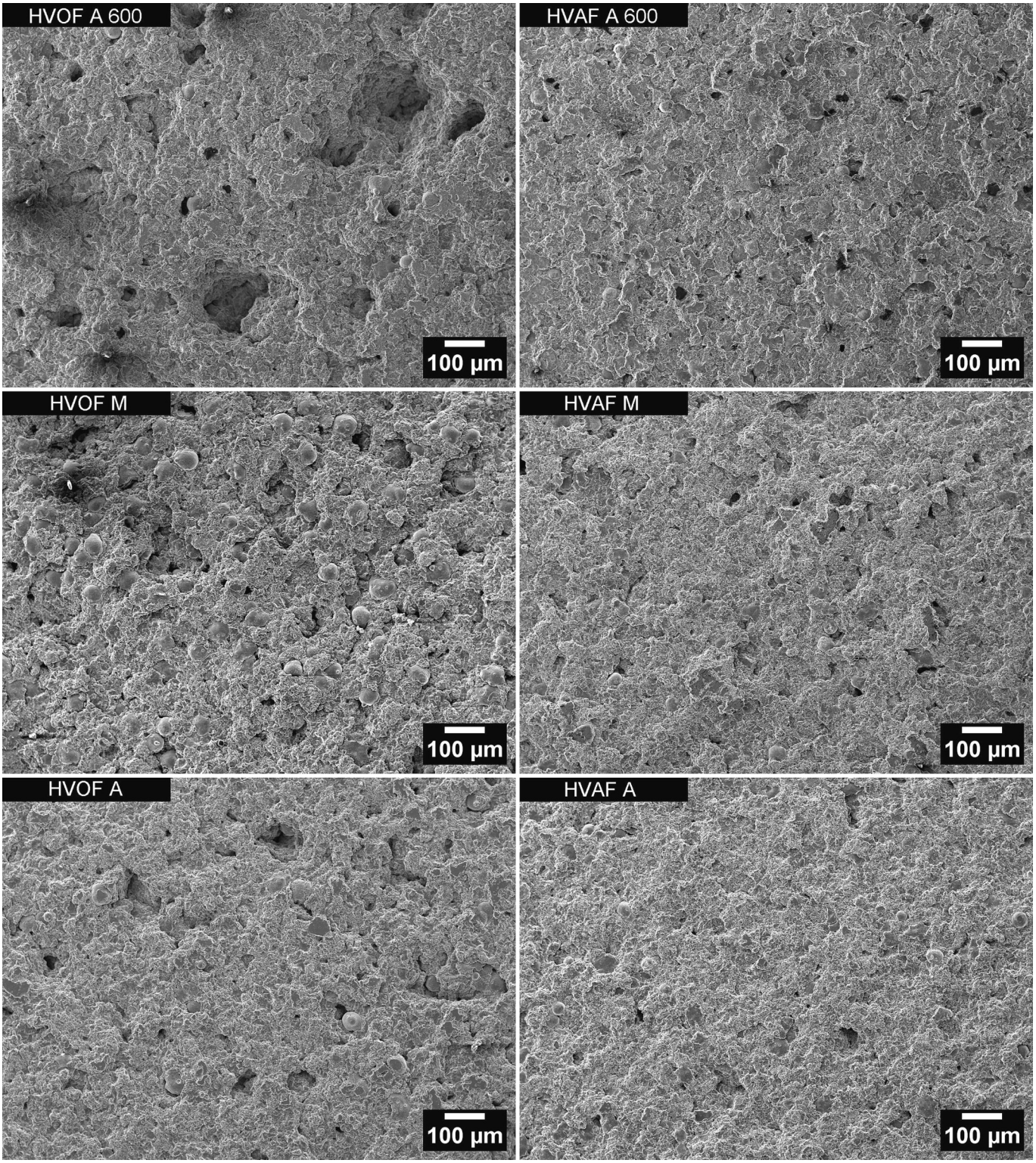

Fig. 11. General view of the cavitation eroded surfaces of the HVOF A, HVAF A, HVOF M, HVAF M, HVOF A600, and HVAF A600 coatings by SEM.

martensitic coatings were in the heat-treated state. The heat treatment can be expected to increase the interlamellar adhesion of the coating, thus improving cavitation resistance. However, it can be noted that the cavitation erosion of the coating on worn surfaces indicated that in some cases crack growth occurred through the lamellae rather than along the lamellae boundaries. At such points, the austenitic phase may prevent crack growth, but this is difficult to prove because other factors in the coating influence its resistance to cavitation erosion. This observation is in line with Lavigne et al. [13].

4. Conclusions

The research questions addressed in this study are a) how the different initial structure of the powder affects the structure of the coating, b) how the different coating methods, HVOF versus HVAF, affect the resulting microstructure, c) how different heat treatments of

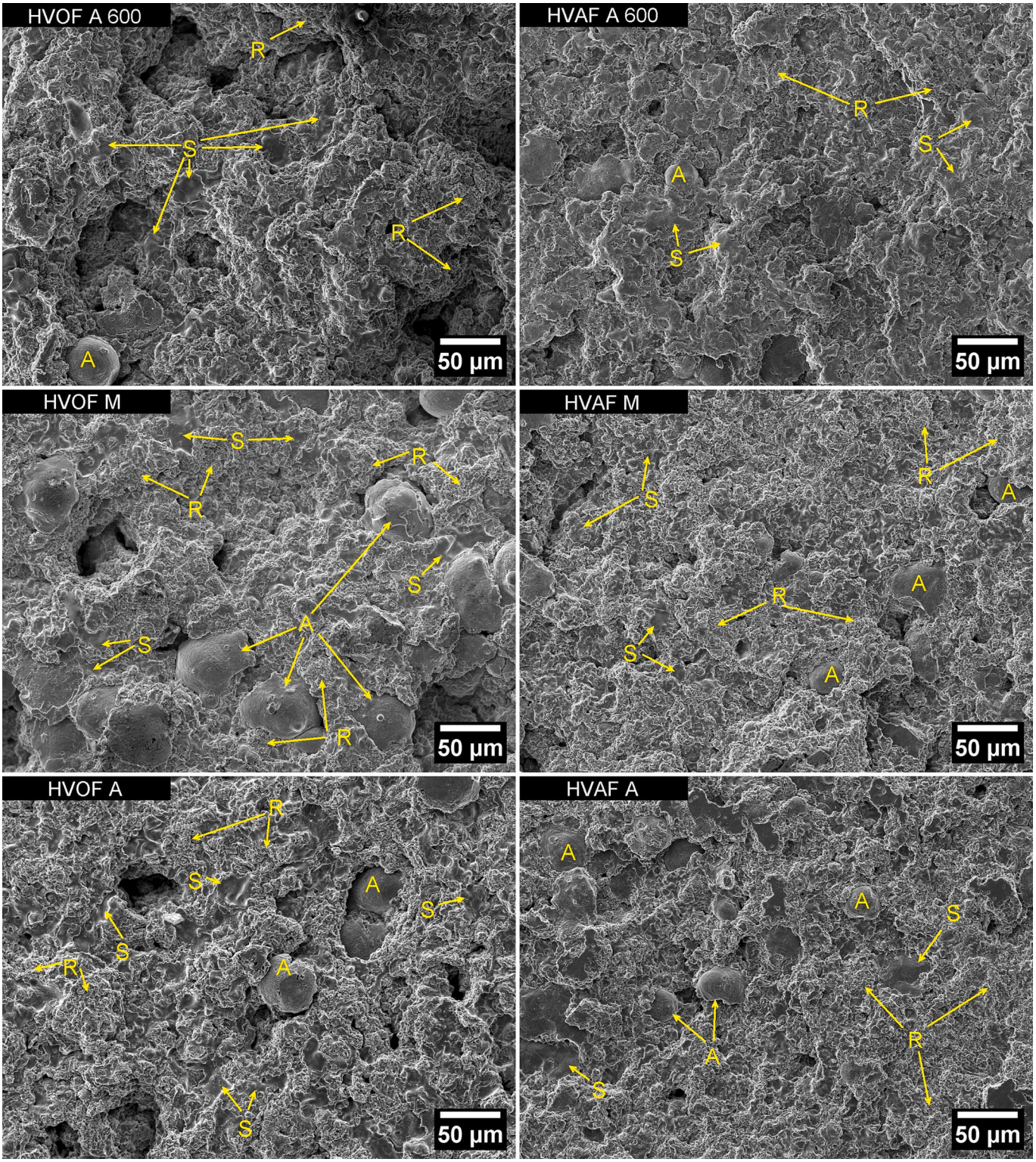

Fig. 12. Detailed cavitation eroded surfaces of the HVOF A, HVAF A, HVOF M, HVAF M, HVOF A600, and HVAF A600 coatings by SEM. The typical features indicated are smooth spotted surfaces (S), non-melted particles (A) and coarse cavitation fracture surfaces due to fatigue (R).

iron-based coatings affect the wear resistance of the coating. Thermal sprayed coatings are characterized by a nonequilibrium and a highly complex microstructure, which clearly makes it difficult to obtain properties through heat treatments and also makes it difficult to assess the influence of different factors on the results obtained. However, the following conclusions were drawn from the results:

- Atomized tool steel powder was found to have a retained austenitic structure with eutectic carbides. The powder was heat treated by annealing at 550 °C, after which the main phase of the powder was martensite. However, the starting phase of the powder did not significantly affect the crystalline structure of the iron in the coating. Both the martensitic and austenitic powders formed a similar,

predominantly retained austenitic supersaturated structure in HVOF and HVAF coatings.

- Abrasion resistance usually depends mainly on the hardness of the surface and the ability of abrasive particles to penetrate the surface. In the case of thermally sprayed iron coatings, no clear correlation was found with the hardness of the coating and the abrasive wear resistance. The abrasion resistance of the coatings was improved only by heat treatment (600 °C) that resulted in the formation of globular larger size carbides.
- It was apparent that cavitation erosion, a type of fatigue wear in which material was removed through a crack growth mechanism, was mainly influenced by the quality of the lamellar interfaces in the coatings. The study highlighted the negative effect of both well-melted, highly on cavities oxidized lamellar interfaces and, on the other hand, poor adhesion of non-melted particles on the cavitation resistance of as sprayed coatings. The quality of the lamellar interfaces explained the significantly better cavitation erosion resistance of HVAF sprayed tool steel coatings compared to HVOF sprayed ones. The adhesion of the lamellae could be improved by heat treatment for HVAF coatings, as there were no brittle oxides at the lamellae boundaries. HVOF coatings suffered from oxides at the lamellar boundaries which reduced the local fracture toughness allowing cracks propagated easily along oxidized interfaces. It was evident that cavitation erosion resistance of such HVOF coatings could not be improved by heat treatment.
- The austenitic phase, which is typically good against cavitation erosion, could not be shown to be the main factor improving the cavitation resistance of thermally sprayed tool steel coatings because other factors such as lamellar boundary properties and oxide inclusions had also significant influence on the cavitation resistance.

CRediT authorship contribution statement

Tommi Varis: Investigation, Conceptualization, Methodology, Visualization, Writing – original draft, Writing – review & editing. **Juha Lagerbom:** Investigation, Conceptualization, Methodology, Visualization, Writing – original draft. **Tomi Suhonen:** Investigation, Conceptualization, Writing – review & editing. **Lassi Raami:** Investigation, Visualization, Writing – review & editing. **Sakari Terho:** Investigation, Methodology. **Jussi Laurila:** Investigation, Writing – review & editing. **Pasi Peura:** Supervision, Writing – review & editing. **Petri Vuoristo:** Supervision.

Declaration of competing interest

The authors declare that they have no known competing financial interests or personal relationships that could have appeared to influence the work reported in this paper.

Data availability

Data will be made available on request.

Acknowledgements

The research was funded by Academy of Finland, project “Enabling phenomena behind multihierarchical strengthening of high kinetic sprayed metallic coatings” (HIERARCH, Decision NUM: 318064). Authors would like to thank Anssi Metsähonkala and Jarkko Lehti from Tampere University, Thermal Spray Center Finland (TSCF), Tampere, Finland, for spraying the coatings and Luka Valmu from Tampere University for carrying out the wear tests.

References

[1] E. Sadeghimeresht, N. Markocsan, P. Nylén, Microstructural characteristics and corrosion behavior of HVAF- and HVOF-sprayed fe-based coatings, Surf. Coat. Technol. 318 (2017) 365–373, https://doi.org/10.1016/j.surfcoat.2016.11.088.
[2] M. Oksa, T. Varis, K. Ruusuvuori, Performance testing of iron based thermally sprayed HVOF coatings in a biomass-fired fluidised bed boiler, Surf. Coat. Technol. 251 (2014) 191–200, https://doi.org/10.1016/j.surfcoat.2014.04.025.
[3] T. Varis, D. Bankiewicz, P. Yrjas, M. Oksa, T. Suhonen, S. Tuurna, K. Ruusuvuori, S. Holmström, High temperature corrosion of thermally sprayed NiCr and FeCr coatings covered with a KCl–K2SO4 salt mixture, Surf. Coat. Technol. 265 (2015) 235–243, https://doi.org/10.1016/j.surfcoat.2014.11.012.
[4] Liu-Xi Cai, Jing-Ru Mao, Shun-Sen Wang, Juan Di, Zhen-Ping Feng, Experimental investigation on erosion resistance of iron boride coatings for steam turbines at high temperatures, Proc. Inst. Mech. Eng. Part J J. Eng. Tribol. 2015 (229) (2015) 636–645.
[5] Y. Wang, Y.G. Zheng, W. Ke, W.H. Sun, W.L. Hou, X.C. Chang, J.Q. Wang, Slurry erosion–corrosion behaviour of high-velocity oxy-fuel (HVOF) sprayed fe-based amorphous metallic coatings for marine pump in sand-containing NaCl solutions, Corros. Sci. 53 (2011) 3177–3185, https://doi.org/10.1016/j.corsci.2011.05.062.
[6] B. Wielage, H. Pokhmurska, T. Grund, S. Ahrens, A. Wank, G. Reisel, T.M. Schnick, E. Deppe, Vanadium-rich iron-based thermal spray coatings for combined wear and corrosion protection, in: B.R. Marple, M.M. Hyland, Y.-C. Lau, R.S. Lima, J. Voyer (Eds.), Seattle, Washington, USA, 2006, pp. 1107–1112, https://doi.org/10.31399/asm.cp.itsc2006p1107.
[7] S. Uozato, K. Nakata, M. Ushio, Evaluation of ferrous powder thermal spray coatings on diesel engine cylinder bores, Surf. Coat. Technol. 200 (2005) 2580–2586, https://doi.org/10.1016/j.surfcoat.2005.05.042.
[8] A. Rabiei, D.R. Mumm, J.W. Hutchinson, R. Schweinfest, M. Rühle, A.G. Evans, Microstructure, deformation and cracking characteristics of thermal spray ferrous coatings, Mater. Sci. Eng. A 269 (1999) 152–165, https://doi.org/10.1016/S0921-5093(99)00132-X.
[9] H. Liborius, A. Nestler, G. Paczkowski, A. Schubert, T. Grund, T. Lampke, Surface integrity in turning of Fe17Cr2Ni0.2C iron based thermally sprayed coatings with special respect to the influence of the feed, MM SJ. 2019 (2019) 3220–3227, https://doi.org/10.17973/MMSJ.2019_11_2019074.
[10] M.S. Priyan, P. Hariharan, The study on tribology and surface Interface characterization of fe based alloy coating deposited by HVOF method, Procedia Eng. 38 (2012) 3741–3756, https://doi.org/10.1016/j.proeng.2012.06.430.
[11] M.S. Priyan, P. Hariharan, Wear and Corrosion Resistance of Fe Based Coatings by HVOF Sprayed on Gray Cast-Iron for Automotive Application 36, 2014.
[12] K. Bobzin, M. Öte, T. Königstein, K. Dröder, H.-W. Hoffmeister, G. Mahlfeld, T. Schläfer, Development of novel fe-based coating systems for internal combustion engines, J. Therm. Spray Technol. 27 (2018) 736–745, https://doi.org/10.1007/s11666-018-0705-3.
[13] S. Lavigne, F. Pougoum, S. Savoie, L. Martinu, J.E. Klemberg-Sapieha, R. Schulz, Cavitation erosion behavior of HVOF CaviTec coatings, Wear 386–387 (2017) 90–98, https://doi.org/10.1016/j.wear.2017.06.003.
[14] A. Kumar, J. Boy, R. Zatorski, L.D. Stephenson, Thermal spray and weld repair alloys for the repair of cavitation damage in turbines and pumps: a technical note, J. Therm. Spray Technol. 14 (2005) 177–182, https://doi.org/10.1361/10599630523737.
[15] R. Singh, S.K. Tiwari, S.K. Mishra, Cavitation erosion in hydraulic turbine components and mitigation by coatings: current status and future needs, J. Mater. Eng. Perform. 21 (2012) 1539–1551, https://doi.org/10.1007/s11665-011-0051-9.
[16] A. Milanti, V. Matikainen, G. Bolelli, H. Koivuluoto, L. Lusvarghi, P. Vuoristo, Microstructure and sliding wear behavior of fe-based coatings manufactured with HVOF and HVAF thermal spray processes, J. Therm. Spray Technol. 25 (2016) 1040–1055, https://doi.org/10.1007/s11666-016-0410-z.
[17] G. Bolelli, B. Bonferroni, J. Laurila, L. Lusvarghi, A. Milanti, K. Niemi, P. Vuoristo, Micromechanical properties and sliding wear behaviour of HVOF-sprayed fe-based alloy coatings, Wear 276–277 (2012) 29–47, https://doi.org/10.1016/j.wear.2011.12.001.
[18] C. Heathcock, B. Protheroe, A. Ball, Cavitation erosion of stainless steels, Wear 81 (1982) 311–327.
[19] S. Hattori, E. Nakao, Cavitation erosion mechanisms and quantitative evaluation based on erosion particles, Wear 249 (2001) 839–845, https://doi.org/10.1016/S0043-1648(00)00308-2.
[20] S. Hattori, R. Ishikura, Revision of cavitation erosion database and analysis of stainless steel data, Wear 268 (2010) 109–116, https://doi.org/10.1016/j.wear.2009.07.005.
[21] M.C. Park, K.N. Kim, G.S. Shin, S.J. Kim, Effects of strain induced martensitic transformation on the cavitation erosion resistance and incubation time of Fe–Cr–Ni–C alloys, Wear 274–275 (2012) 28–33, https://doi.org/10.1016/j.wear.2011.08.011.
[22] G.S. Shin, J.Y. Yun, M.C. Park, S.J. Kim, Effect of mechanical properties on cavitation erosion resistance in $\gamma \rightarrow \alpha'$ phase transformable Fe–Cr–C–Mn alloys, Tribol. Lett. 57 (2015) 25, https://doi.org/10.1007/s11249-015-0468-7.
[23] J.Y. Yun, G.S. Shin, M.C. Park, H.S. Lee, W.S. Kang, S.J. Kim, Effect of strain-induced ε and α′-martensitic transformation on cavitation erosion resistance in austenitic fe-cr-C-MnFe–cr–C–Mn-ti alloys, Wear 338–339 (1915), 379384.
[24] P. Niederhofer, S. Huth, Cavitation erosion resistance of high interstitial CrMnCN austenitic stainless steels, Wear 301 (2013) 457–466, https://doi.org/10.1016/j.wear.2012.12.050.

[25] A. Rajput, J. Ramkumar, K. Mondal, Cavitation behavior of various microstructures made from a C-mn eutectoid steel, Wear 486–487 (2021), 204056, https://doi.org/10.1016/j.wear.2021.204056.
[26] A. Milanti, H. Koivuluoto, P. Vuoristo, G. Bolelli, F. Bozza, L. Lusvarghi, Microstructural characteristics and tribological behavior of HVOF-sprayed novel fe-based alloy coatings, Coatings 4 (2014) 98–120, https://doi.org/10.3390/coatings4010098.
[27] W. Yuping, L. Pinghua, C. Chenglin, W. Zehua, C. Ming, H. Junhua, Cavitation erosion characteristics of a Fe–Cr–Si–B–Mn coating fabricated by high velocity oxy-fuel (HVOF) thermal spray, Mater. Lett. 61 (2007) 1867–1872, https://doi.org/10.1016/j.matlet.2006.07.147.
[28] A. Milanti, H. Koivuluoto, P. Vuoristo, Influence of the spray gun type on microstructure and properties of HVAF sprayed fe-based corrosion resistant coatings, J. Therm. Spray Technol. 24 (2015) 1312–1322, https://doi.org/10.1007/s11666-015-0298-z.
[29] G. Bolelli, T. Börner, A. Milanti, L. Lusvarghi, J. Laurila, H. Koivuluoto, K. Niemi, P. Vuoristo, Tribological behavior of HVOF- and HVAF-sprayed composite coatings based on fe-Alloy+WC–12% co, Surf. Coat. Technol. 248 (2014) 104–112, https://doi.org/10.1016/j.surfcoat.2014.03.037.
[30] R. Colaço, R. Vilar, On the influence of retained austenite in the abrasive wear behaviour of a laser surface melted tool steel, Wear 258 (2005) 225–231, https://doi.org/10.1016/j.wear.2004.09.029.
[31] S. Martin, S. Wolf, U. Martin, L. Krüger, D. Rafaja, Deformation mechanisms in austenitic TRIP/TWIP steel as a function of temperature, Metall. Mater. Trans. A 47 (2016) 49–58, https://doi.org/10.1007/s11661-014-2684-4.
[32] G.F.V. Voort, Martensite and retained austenite, Ind. Heat. 76/4 (2009) 51–54.
[33] P. Delshad Khatibi, H. Henein, A.B. Phillion, Microstructure and mechanical characterization of rapidly solidified cr-C tool steel: annealing effects, Adv. Powder Technol. 27 (2016) 2076–2083, https://doi.org/10.1016/j.apt.2016.07.019.
[34] A. Röttger, S. Weber, W. Theisen, B. Rajasekeran, R. Vassen, Mechanical properties of thermally sprayed fe based coatings, Mater. Sci. Technol. 27 (2011) 973–982.
[35] R.K. Sharma, R.K. Das, S.R. Kumar, Microstructure, mechanical and erosion wear analysis of post heat treated iron alloy based coating with varying chromium, Mater. Werkst. 52 (2021) 1173–1184, https://doi.org/10.1002/mawe.202100080.
[36] G. Liu, Y. An, J. Chen, G. Hou, J. Chen, Influence of heat treatment on microstructure and sliding Wear of thermally sprayed fe-based metallic glass coatings, Tribol. Lett. 46 (2012) 131–138.
[37] W.-H. Liu, F.-S. Shieu, W.-T. Hsiao, Enhancement of wear and corrosion resistance of iron-based hard coatings deposited by high-velocity oxygen fuel (HVOF) thermal spraying, Surf. Coat. Technol. 249 (2014) 24–41, https://doi.org/10.1016/j.surfcoat.2014.03.041.
[38] D. Poirier, Y. Thomas, B. Guerreiro, M. Martin, M. Aghasibeig, E. Irissou, Improvement of tool steel powder cold sprayability via softening and agglomeration heat treatments, J. Therm. Spray Technol. 31 (2022) 145–158, https://doi.org/10.1007/s11666-022-01320-4.
[39] J. Valloton, D.M. Herlach, H. Henein, D. Sediako, Microstructural quantification of rapidly solidified undercooled D2 tool steel, Metall. Mater. Trans. A 48 (2017) 4735–4743, https://doi.org/10.1007/s11661-017-4249-9.
[40] J. Stella, M.R. Cruz, J. López, Cavitation erosion and sliding Wear to assess carbide integrity in AISI D2 tool steel, Tribol. Lett. 51 (2013) 49–56, https://doi.org/10.1007/s11249-013-0144-8.